Earthen construction: an increase of the mechanical strength by optimizing the dispersion of the binder phase

Mariette Moevus · Yves Jorand · Christian Olagnon · Sandrine Maximilien · Romain Anger · Laetitia Fontaine · Laurent Arnaud

Abstract Although of interest for its low embodied energy content for construction, earth is usually not used for modern construction due to the expensive, artisanal and complicated process and the high variability of the raw material. The transfer of techniques dedicated to cement concrete could help the industrialization of this material. The use of dispersant for an improved dispersion of the earth powder has been investigated for both dispersion of earth fine fraction and water (here named the binding phase) and mortar made with calibrated sand. An improvement of the rheology is observed with lower viscosity and yield stress. This leads to a very small improvement of the density however concomitant with a marked increase of the mechanical properties, Young modulus and compressive strength. The analysis of the microstructure of the mortar shows an increase of the largest pores, and a decrease of the clay platelets flocs. The evolutions of these properties are analyzed in terms of the Rumpf model at two different scales. The dispersant mainly acts on the platelet arrangement that defines the forces between particles, but also simultaneously decreases the permeability of this binding phase, therefore entrapping more air during the mixing of the powder and water. Clearly the use of a dispersant may be of interest for the processing of earth material on liquid state, decreasing the viscosity and/or allowing the reduction of the water content, and finally improving strength.

Keywords Earth construction · Strength · Dispersants · Clays · Fluidification

M. Moevus · R. Anger
Les Grands Ateliers, Boulevard de Villefontaine,
38092 Villefontaine, France
e-mail: mariette.moevus@lesgrandsateliers.fr

R. Anger
e-mail: romain.anger@lesgrandsateliers.fr

Y. Jorand (✉) · C. Olagnon · S. Maximilien
MATEIS, INSA Lyon, Université de Lyon, 20 Avenue
Albert Einstein, 69621 Villeurbanne, France
e-mail: yves.jorand@insa-lyon.fr

C. Olagnon
e-mail: christian.olagnon@insa-lyon.fr

S. Maximilien
e-mail: sandrine.maximilien@insa-lyon.fr

L. Fontaine
Ecole Nationale Supérieure d'Architecture de Grenoble,
Université de Grenoble, 60 Avenue de Constantine,
CS 12636, 38036 Grenoble, France
e-mail: laetitia.fontaine@grenoble.archi.fr

L. Arnaud
Ecole Nationale des Arts et Metiers, Rue Porte de Paris,
71250 Cluny, France
e-mail: laurent.arnaud@ensam.eu

1 Introduction

Nowadays, the use of cement based concrete for housing has almost become the hegemonic solution. It presents several simultaneous advantages such as ease of processing complicated shapes by molding, and achieving a high, robust and reliable strength. Recent progress has lead to high performance concretes allowing reducing structure thickness [1, 31]. Nevertheless, it exhibits several drawbacks such as a low hydraulic transport leading to moisture problems in buildings, and low thermal inertia [16, 32, 36, 37]. In addition, these last years studies on carbon accounting have exhibited the high-embodied energy content due to cement production and transport when not locally produced. Moreover, the high mechanical properties of this material are very large compared to the needs in terms of real solicitation in standard housing.

Earth has been widely used as a traditional material all over the world. It appears a sustainable material since many ancient buildings are still used after several centuries, but the different processes are based on artisanal and local knowledge. There has been however for a few years a renewed interest in this material, even in developed countries [19, 24, 35] where major architects have proposed appealing modern constructions. Therefore, the development of this material is limited by technical difficulties preventing industrialization of the process. Until now, earth construction is mostly achieved by processes implying compaction of low water content mixtures.

One alternative way to promote earth construction could be to use a similar process as cement-based concrete that could be molded and dried over one day. There are two main scientific barriers to solve this challenge. The first one is the non-existence of a hydraulic binding phase in raw earth; the hardening is caused by drying. But the drying duration after molding is too long and prevents a remolding over typically one day. The second one is a low reliability of the properties, owing to the variability of the raw materials. This paper addresses mostly the second point, i.e. understanding and improving the mechanical properties.

The simplest model relating the strength to granulated material that takes into account its porosity was proposed by Rumpf and coworkers [39], the mechanical behavior of granular compacts is linked to the packing density, i.e. the number of contacts, and the energy of the contacts. Rumpf has proposed that the mechanical tensile resistance of a compact is:

$$\sigma_t = \frac{1-P}{P}\frac{f}{d^2},$$

where P is the porosity, f is the mean tensile force per contact and d the diameter of the particles. The factor $(1-P)/P$ represents the contribution of the packing organization, $\phi = 1 - P$ is the packing density related to the coordination number. The basic idea of the model is that the strength is the sum of the forces of contacts in the rupture plane, which is simplified since rupture rather starts at one point before propagation. However, different refinements [23, 44] lead to results sufficiently close to use this conceptual simple model in order to obtain a first order approximation of the mechanical behavior. It initially describes the behavior of spheres of unique diameter submitted to Van der Waals attraction, but has also been extended to assemblies of particles submitted to other forces such as capillarity [12]. This simple model can be applied to a construction material, considered as aggregates, linked by a binder phase (cement, clays, plaster…). It shows that the strength can be improved either by increasing the packing density, which is commonly done by a specific design of the particle size distribution [2, 4], for the pioneer authors) or by increasing the binding force between construction aggregates. In earth-based construction materials, Henri Van Damme [21] has suggested that it is possible to increase the bond strength, f, by improving organization of the particles in the clay-based binding phase. In a processing route (poured earth) where a liquid state must be achieved, the use of a relevant dispersant to improve the dispersion stability might be a way to reach this objective.

In this paper we have considered a simplified earth construction material considering a model mortar consisting of a skeleton of sand particles (representing the construction aggregates), embedded in a so-called binder phase constituted of the fine fraction of a real earth (mainly containing clays). Inconsistencies exist in the literature on the definitions of terms related to divided materials, partly because different disciplines have their own use ([7, 33], for example). In order to avoid confusion, the terms used in this paper are clearly specified in the experimental part. The idea of the present work is to show and understand the effect

of a dispersant on the mechanical behavior of a model mortar based on clay binder and normalized sand.

2 Experimental methods

2.1 Materials

As mentioned above, we have decided to define a model material, simpler and more reliable in order to simplify the understanding. We consider the fine part of soil as the binding phase in earth-based building materials. In order to enhance the effect of the dispersant on the rheology we have prepared suspensions with only the binding phase, i.e. without sand. However, it is not possible to make non-cracked compacts of reasonable size with only the binding phase. We have therefore also prepared a model mortar, by adding normalized siliceous sand (EN 196-1) to assess the mechanical properties.

2.1.1 Binding phase

The raw material is a soil extracted from a carrier in Dauphiné (France). This soil is suitable for rammed earth construction. It was sieved at 100 µm and the passing is considered as the binding phase. The density measured by helium pycnometry is equal to 2590 kg m^{-3}. X-ray diffraction qualitative analysis shows the presence of clays (illite and muscovite), and tectosilicates (albite, microcline and quartz). The particles size distribution obtained by sieve analysis and sedimentometry is shown in Fig. 1.

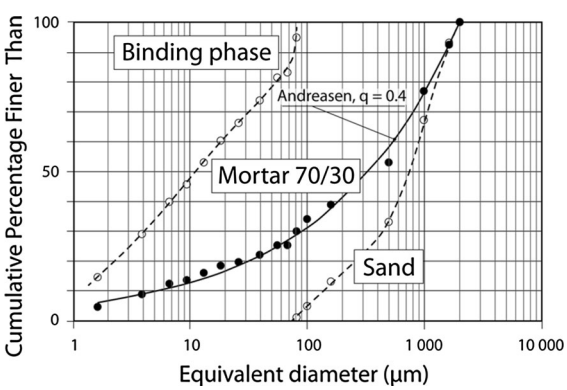

Fig. 1 Cumulative particule size distribution of the sieved soil, the sand and the 70/30 mix. The solid line corresponds to the theoretical model of Andreassen with an exponent of 0.4

2.1.2 Mortar

We have defined optimized mortar samples in order to (i) minimize the shrinkage induced by drying the specimens, (ii) increase the final density and (iii) minimize the water ratio required for processing. This has been achieved by mixing sieved soil and sand of controlled granulometry. We considered the continuous distribution of the Andreassen theory [3] expressing the distribution as:

$$F(d) = (d/d_{\max})^q$$

where F represents the cumulative fraction of particles finer than d, $d_{\max}$ the maximum particle size and q a parameter defining the width of the distribution. It is assumed that a value of q between 0.2 and 0.5 leads to the highest packing density. We have selected the fraction of both components such that the Andreasen coefficient was in that range, which lead to 30 wt% of sieved soil and 70 wt% of sand. The final size distribution has been calculated from the measured distributions according to:

$$F(d) = 0.3 \times F_{\text{soil}}(d) + 0.7 \times F_{\text{sand}}(d)$$

and fitted to the Andreasen model, which gives an exponent value of $q = 0.4$, with a good fit (Fig. 1).

A precise sample preparation protocol has been defined to make cylindrical specimens. A quantity of 579 g of sieved soil is mixed in a mortar planetary mixer with 300 g of purified water (resistivity $\geq$ 10 MΩ), and with the eventual dispersing agent for 1 h. This highly viscous slurry is sealed in a plastic bag and stored at 20 °C for 24 h. It is subsequently put back in the mixer bowl with 1350 g of sand and stirred for 5 min. The process with this type of material can be done either at constant water to solid ratio or at constant consistency. We have selected the latter, since it implies constant workability, closer to real situation and simplifies the processing of the powders to shaped specimens. The consistency of the dispersion is measured on a flow table (a standard tool in civil engineering giving a measure of the consistency), where the required value is a spreading diameter of 15.5 ± 0.5 cm after 15 drops. When the diameter is two small, some water is added until the desired value is obtained. The slurry is then poured in one step in the cylinder moulds (30 mm diameter and 60 mm height) of surfaces lubricated

with silicon oil. The moulds are subsequently submitted to 30 drops on the same flow table. The moulded samples dry for one night, then are put upside down in order to allow the other face to dry for 1 day. The samples are removed from their moulds around 40 h after having been cast so that some drying shrinkage arises allowing the specimen surfaces to disjoint the mould. The specimens are subsequently stored at 20 °C under controlled humidity of 50 % R.H. for 1 week. The apparent density was evaluated on the cylindrical specimen from the weight and the volume measured by a calliper.

2.1.3 Dispersants

Among the wide choice of potential dispersing agents to stabilize clay dispersions we selected the sodium hexametaphosphate (Na-HMP) and a polyacrylic acid with Na^+ side groups (PAAS). Sodium hexametaphophate is a widely used dispersant, known as a surface complexant, in traditional ceramic processing and for particle size analysis of soils (ASTM D422-63). It combines an "electrostatic" mechanism and a sequestering action toward Ca^{2+} flocculating cations. Nevertheless, the main contribution seems to come from the first mechanism. For oxide particles, Andreola et al. [5] reports that the strong adsorption of the phosphate anions onto surface positive sites increases the net negative charge of the surface. When added to clay-based products, Na-HMP adsorbs on edge positive alumina sites [45], decreasing the values of yield stress and apparent viscosity, overcoming the edge-to-edge attractive interactions.

Polyacrylic acids are polyelectrolyte dispersants widely used, especially in ceramic industry. They combine electrostatic and steric effects. This results in an increase of the edge-to-edge repulsive interaction, promoting the switching of coagulated clays systems from an edge-to-face to a face-to-face configuration [45, 46]. PAA polymer are adsorbed on surface oxides by means of a strong electrostatic interaction of acrylic acid groups with the positive sites surface [11, 46] and, in water, the dissociation of the chains, characterized by a pKa close to 4, causes an increase of the negative net particle charge that constitutes the electrostatic effect. Then, if the adsorption ratios are higher with more acidic pH than the zero charge point, the degree of dissociation has also a large incidence on the efficiency of the dispersant. This implies to work in a limited pH range. For alumina dispersions, it has been shown that PAA produces significant effects when pH is in the range from 6 to 11 [8, 15, 38] The molecular weight of the polymer has also a wide incidence. It must be chosen according to the size of the particles to be dispersed. If nanosized oxides particle are employed, the molar weight (M_w) in the order of 2000 g/mol appears to be the most efficient [14, 40]. Similar results are obtained for clay-based products and the best results, for various polyelectrolytes, are obtained when M_w lies between 1200 to 4000 g/mol [13, 26, 46]. The M_w of 2000 g/mol for the PAA used here is in keeping of with theses observations.

2.2 Rheological measurements

The effects of dispersant addition on the rheological behavior are observed with a co-axial rheometer under controlled shear rate (Haake VT 501) on dispersions of the binding phase in water with a solid ratio of 0.361 (60 wt%). This high concentration is chosen in order to be representative of that of an earth concrete. In a first step, the dispersant is dissolved in high purity water (resistivity $\geq$ 10 MΩ) and the solution is homogenized for 3 min. Then the powder is added in small increments while the dispersion is homogenized with a magnetic stirrer. Stirring is maintained during a mellowing period of 24 h before measurements. This duration is chosen on the basis of preliminary results that have shown a reduction of the viscosity evolution with time. This procedure was strictly reproduced for each sample, since small variations may have a large incidence on the state of the dispersion and so its rheological behaviour. The shear rate-time cycle applied consists of an increase from 0 to 1000 s^{-1} in 90 s (reduced to 500 s^{-1} when no dispersant is added since viscosity becomes too high for rheometer capability), followed by a constant shear rate during 30 s. Then shear rate is reduced to 100 s^{-1} in 60 s. After maintaining the shear rate for 30 s, it is decreased to 0 s^{-1} in 30 s. The effect of the dispersant ratio is evaluated using a time-average apparent viscosity during the 100 s^{-1} step when stabilization is reached. Since solid loading may have a large incidence on viscosity, its value is systematically checked by desiccation in an oven at 105 °C after each measurement.

2.3 Mechanical tests

In order to achieve relevant compression tests the sample surfaces are prepared by depositing thin layers of a mortar of fine earth (smaller than 100 µm) stabilised with 16.6 wt% of plaster of Paris. The samples are put back in the mould and the fine mortar is deposited on the first face and carefully flattened with a screed to obtain a surface perpendicular to the cylinder axis. When this mortar is hard, the sample is taken out and deposited up side down on a 1 mm spacer and the same procedure is applied to the second face. In the end both surfaces are parallel and smooth. The compression samples are further stored at 20 °C under 50 % R.H.

The samples are not tested until a constant weight is measured, suggesting water equilibrium. They are taken out of the control humidity chamber, weighed; their length and diameter are measured with a calliper, and sealed in a plastic bag until making the test. An Instron 8562 electromechanical testing machine is used at imposed crosshead displacement rate of 0.004 mm s^{-1} (the duration of a test to rupture is about 5 min), in order to obtain a control rupture behind the peak stress value. A steal half sphere is put between the specimen and the machine plate in order to compensate an eventual parallelism deviation of the specimens. A lubricated plastic thin film is deposited between the specimen surfaces in order to avoid or limit any friction at the specimen boundary and therefore limiting any localised stresses. The strain is directly measured by a 25 mm contact extensometer clipped on the specimen by rubber bands. Therefore the machine stiffness or the increasing stiffness of the half sphere does not affect the measurement.

The engineering fracture strength ($\sigma_r = F_r/S_o$ with F_r the maximum load and S_o the initial normal cross-section area) and the apparent elastic modulus were deduced from the load-strain curve. After mechanical testing the compression samples are dried at 105 °C for at least 3 days in an oven for measuring the residual water content.

2.4 Microstructural characterization

In the present work we propose to describe the microstructure of the material by considering three different characteristic lengths (cf. Fig. 2) each corresponding to a porosity size range. The macroscopic scale (2–30 µm) corresponds to the sand particle sizes, the considered porosities in this range are mainly due to shaping (occluded air, cracks…). The microscopic

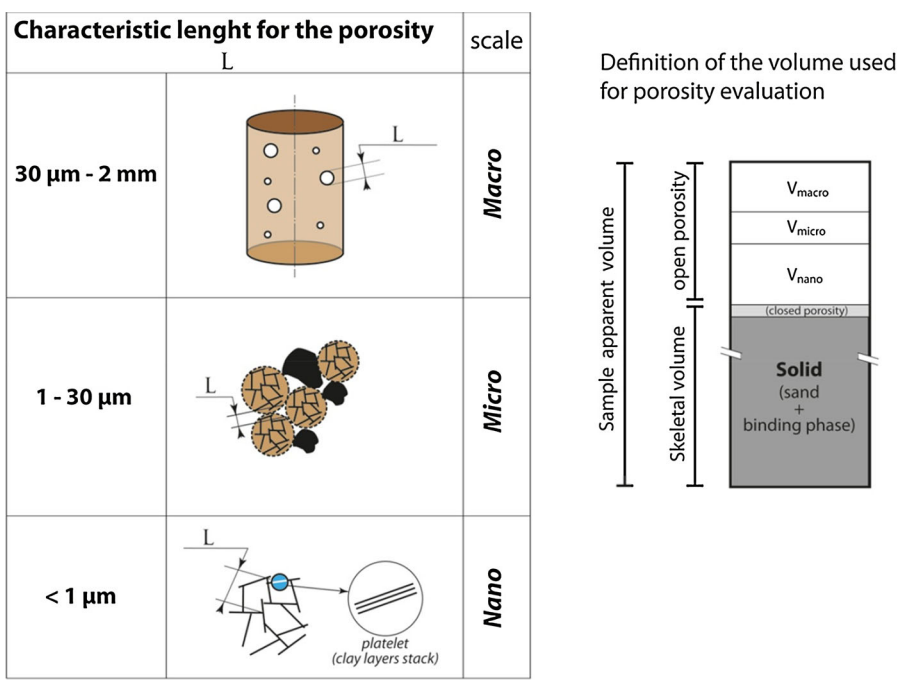

Fig. 2 Schematic drawing illustrating the three scales for the interpretation of the microstructure evolutions

scale (30–1 μm) corresponds to the spaces between the agglomerates of clay particles (particles also called platelets) and of other "associated minerals" [7]. The nanometric scale (below 1 μm) corresponds to voids within the aggregates of clay particles.

2.4.1 SEM analyses

The microstructural organisation of mortars is complex and therefore difficult to analyse. Indeed, even with the small sand grains (2 mm) selected here, the difference of size between the sand and the clay particles is very large. Moreover, it is not possible to cut a sample in order to observe the fracture surface since fracture surely modifies the local microstructure. We have therefore prepared specific specimens for SEM observations.

A drop of mortar suspension was deposited on an aluminium plate and let dry at room temperature. The observations were further conducted under high vacuum at low accelerating voltage (1 kV). This allowed observing the organisation of the clay platelets around the sand particles. However, since it is difficult to observe the influence of the dispersant, we have also prepared samples of pure clay suspension, i.e. without sand, using the same procedure.

2.4.2 Mercury intrusion porosimetry (MIP)

In order to quantify and compare the pore-network of the samples and to complete the analysis by tomography, mercury intrusion porosimetry has been used. This technique is very useful to investigate the pores between 3.5 nm and 500 μm if we keep in mind the numerous assumptions which are made, as well as the closed pores are not accessible [22]. A Micromeritics Autopore 9420 was used. Samples were dried in an oven at 55 °C until constant weight (typically several days). This procedure was intended to limit the degradation of the pore structure during drying. Indeed, Gallé has evidenced an important degradation during the removal of evaporable pore water on cement-based materials [20], and this procedure could be optimised. The weight of each sample was about 3 g. A penetrometer cell with a useful volume of 5 cm^3 was chosen. After removing air, the cell was filled with mercury. The pressure is applied from 0.035 MPa to 414 MPa. The incremental mode is used, with an equilibrium time of 10 s for each measurement value with the standard Micromeritics pressure table.

Intrusion pressure values were directly converted into the corresponding pore interconnection diameter ($2R$) by using the Washburn equation:

$$R = \frac{-2\gamma \cos\theta}{P}$$

with P the mercury intrusion pressure, $\gamma = 0.485$ N m^{-1} the surface tension of mercury and $\theta = 130°$ the contact angle between the solid and mercury. The standard Micromeretics correction factor taking into account the thermoelastic coefficients of cell and mercury has been applied. The results are presented in terms of $\Delta V/(-\Delta \ln d)$ versus $\ln d$, where ΔV is the intrusion volume variation between two pressure points and d the pore interconnection equivalent diameter, as recommended by Moro [30] and Webb and Orr [43] in order to obtain a more representative distribution.

2.4.3 Tomography

X-ray microtomography (V/tome/x, Phoenix X-ray company) was applied at two different resolutions in order to obtain different informations. The tomograph used is presented in [9]. A low resolution of 40 μm was selected to scan the whole cylinders processed for mechanical tests. Such a fast measurement (roughly 5 min per specimen) allowed us to check that no macro defect or microcrack (of typically 1 mm) were present in the sample, or at the interface with the fine mortar. Measurements at a higher resolution of 7 μm were also done on several specimens, again before testing them in order to analyse the porosity distribution in the material. For this purpose the images must be calibrated in terms of contrast/brightness in order to apply the same process. A 3 pixel radius median filter has been applied to reduce the noise, before binarisation with a constant threshold. Two series of erosion/dilatation processes were subsequently applied and the porosities were counted.

2.4.4 Density measurement

The measurement of density on porous materials is difficult, owing to the access of the porosity and to the definition of the measured volume. Therefore in addition to the technique of MIP the density of the

mortar specimens was measured by the so-called Archimedes method, the porosity volume being measured on impregnated materials (derived from a method proposed by Arthur [6]). For this purpose, the specimens are degassed then impregnated by an alkane (density of the alkane were precisely measured to a precision of 10^{-4}) under vacuum. The material effective density is measured on powders by helium pycnometry (Micromeretics, accupyc 1330), after being oven-dried for 24 h at 105 °C. The powders were inserted in the measurement cell at this temperature in order to avoid any moisture adsorption, and cell is purged with helium while cooling to RT temperature. At least ten values are recorded after stabilization.

Clearly the porosity values obtained from both methods are generally different. However, the variations due to the addition of dispersant should be similar, which would reinforce the confidence on the results.

3 Results and discussion

3.1 Rheology of the binding phase

The influence of the addition of different contents of PAAS dispersant on the rheological behaviour of the binding phase is displayed in Fig. 3 in terms of shear stress versus strain rate. Note that the same evolution of the rheological behaviours is observed when Na-HMP is employed instead of PAAS. This is interesting for an application point of view, since it may suggest that the type of dispersant is of less importance. A good fit of the flow curves (descending curves) was obtained with the Casson's model and the yield stress τ_0 and the infinite viscosity η_∞ are displayed in Table 1.

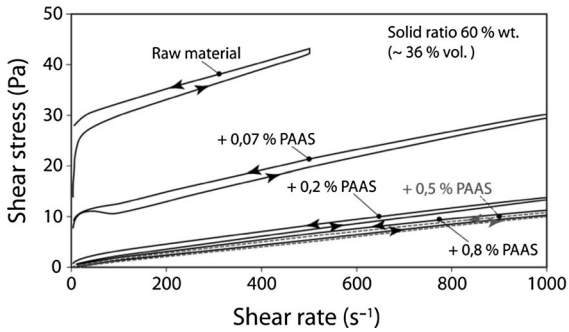

Fig. 3 Rheograms, in terms of shear stress versus shear rates for the binding phase dispersions in water with different PAAS ratios. Note that the evolutions are similar when HMP dispersant is used

The slurry without dispersant shows a pseudo-plastic behaviour associated to a marked anti-thixotropy. As PAAS (or Na-HMP) is added, the yield stress and the loop area between rising and descending curves decreases, i.e. the flow becomes nearly Newtonian, as seen on the evolution of the Casson's yield stress decreasing from about 5 Pa to almost 0. The evolution of the apparent viscosity at 100 s^{-1} versus the dispersant ratio, given Fig. 4, is used to determine the optimum value which reduces the viscosity. A significant viscosity reduction is observed with small dispersant amounts, but once 0.2 % d.w.b. the change becomes negligible.

In dispersions involving equiaxed particles, the occurrence of a pseudo-plastic behaviour indicates a flocculated state. As shear rate increases, an increasing number of flocs are destroyed while the kinetics of their formation remains constant. At sufficient high shear rates particles are all individualized, more liquid is available for flow, the apparent viscosity is significantly reduced. If the attractive forces between particles are replaced by repulsive one, by mean of an "electrostatic" or "steric" stabilization, flow curves evolve towards a quasi-Newtonian behaviour, since little or no floc destruction can occur. Thus flow curves are a clear picture of the dispersion structure [34, 41].

The particles of clay dispersion can be seen as platelets with edges and faces of different surface chemistry. This can lead to a much more complex evolution of their rheological behaviour. Nevertheless, a pseudo plastic flow curve is also related to

Table 1 Evolution of the Casson's parameters with the dispersant ratio (% dwb)

	Na-HMP		PAAS	
	τ_0 (Pa)	η_∞ (mPa s)	τ_0 (Pa)	η_∞ (mPa s)
0 %	4.90	63	4.90	63
0.07 %	2.28	86	2.74	85
0.2 %	0.04	96	0.47	100
0.5 %	0.05	85	0.14	99
0.8 %	0.09	93	0.09	97

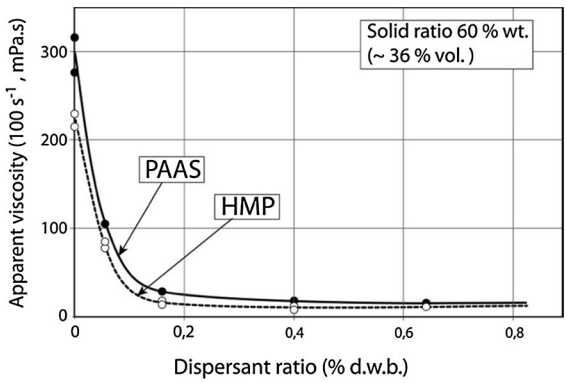

Fig. 4 Evolution of the apparent viscosity at a constant shear rate of 100 s^{-1} as function dispersant ratios

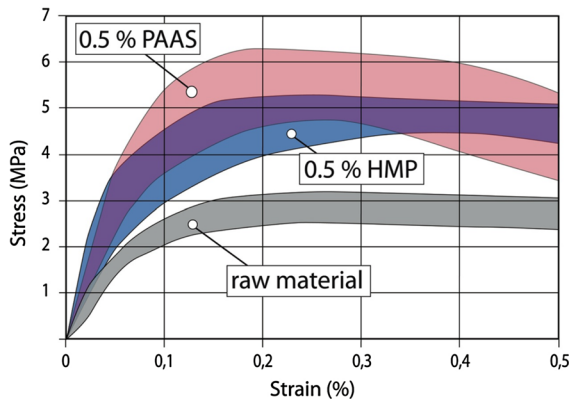

Fig. 5 Envelopes of the stress–strain curves of the mortars without dispersant and with the optimum ratios of both studied dispersants (determined from the optimum plateau of Fig. 3)

destruction of house cards flocs structure to platelets individualization [25].

The occurrence of an anti-thixotropic behaviour is however unexpected. Indeed, pseudo-plastic flow curves are generally associated to thixotropy, since both floc destruction and initial fluid structure recovery, as shear rate is suppressed, are time dependant. Anyway, similar observations have already been reported for kaolin or illite based dispersions. But it seems that the origin of this behaviour remains quite unclear and open to discussion [27, 29].

3.2 Mechanical behavior

Three mortars have been prepared. One, without dispersant (for reference) and two with 0.5 wt% of PAAS and HMP respectively. Figure 4 shows that a lower content of 0.2 wt% would have been enough since the viscosity already reached the plateau. However, owing to the inherent variability of such earth materials, a higher quantity, making the process more robust was selected. The quantity of mixing water to obtain the target consistency (therefore for the same workability) is respectively 15.1, 13.2 and 12.4 wt%. Clearly the caution used for preparing the specimens and conducting the mechanical tests was relevant, since albeit the inherent scattering of such tests for such materials, the effect of dispersant is clear. We have plotted in Fig. 5 only the envelope of the stress–strain curves, and reported the mean values in the Table 2. The compositions with PAA and without dispersant have been processed with a different operator (so-called batch 2) to ensure the reproducibility of the results and 10 mechanical samples tested without extensometer to obtain the strength. The addition of a dispersant, associated to the reduction of the water content is concomitant with an increase of the mechanical properties in terms of strength and elastic modulus, of 50 to 100 % for PAAS and from 40 to 100 % for HMP. The dry density (Table 2) also slightly increases with the addition of a dispersing agent at the mixing stage. The variation is small but larger than the scattering.

3.3 Microstructures

Figure 6 shows slices of typical microstructures obtained from high-resolution tomography (voxel volume of 343 μm^3). In the originals slices (Fig. 6a), the aggregates and the binding phase appear with intermediate grey levels, depending on their composition and porosities in black. It is somewhat surprising that the qualitative observation of these slices shows a higher fraction of large porosities when a dispersant is added. The quantitative analysis of the pore size distribution is performed on binarized and treated slices such as the typical examples given in Fig. 6b. The distribution is calculated in terms of number of pores per volume unit versus the volume equivalent diameter. The resulting pore size distribution of 3 samples prepared without dispersant and with 0.5 % of PAAS are given in Fig. 7. Note that the distribution is truncated at an equivalent diameter of 30 µm. Below this equivalent diameter, large erratic fluctuations are observed, which indicates that under about 41 voxels the noise in the image distorts the analysis.

Table 2 Summary of the densities and mechanical properties

Dispersant	Batch	ρ_{dry} (g/cm^3)		f_c (MPa)		E (GPa)	
		Mean	SD	Mean	SD	Mean	SD
No	1	2.02	0.03	3.23	0.17	4.5	0.4
	2	–	–	3.1	0.4	–	–
0.5 % PAA	1	2.07	0.01	6.08	0.23	7.6	0.8
	2	–	–	6.00	0.1	–	–
0.5 % HMP	1	2.10	0.03	5.12	0.23	7.0	1.9

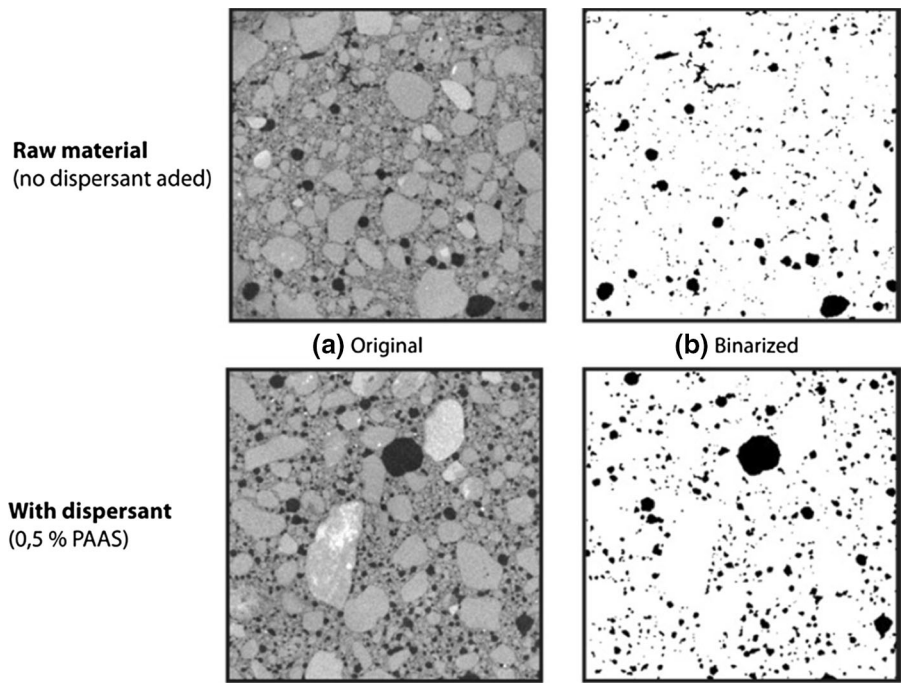

Fig. 6 Microtomography analysis of the microstructure for mortars without and with 0.5 PAAS showing slices of (**a**) an original grey level image and (**b**) a processed binarized image for quantitive pore analysis

The three distributions of each sample type are very close, so at this scale the microstructure is reproducible and its analysis reliable. The quantitative results confirm the qualitative observation, and shows that dispersant addition increases the number of the largest pores, in the range of 50 to about 300 μm in equivalent diameter. We suppose that this microstructure evolution comes from the mixing step. One of the goals of this operation is to remove the entrapped air of the initial granular materials. As we have supposed that dispersant addition induces a more orderly structure of clay platelets in the binding phase, then it can be assumed that the permeability of the mortar is reduced and so its capability to evacuate the entrapped air. This evolution of clay permeability with dispersant addition has previously been observed [29], it is also a part of the know-how of traditional ceramics which indicates that slurries used for filtration casting must not be prepared at the optimum dispersant ratio to avoid long processing time.

Figure 8 shows the results of mercury intrusion porosimetry (MIP) conducted on three samples of both materials without dispersant and with PAA. The different experimental points have been plotted and

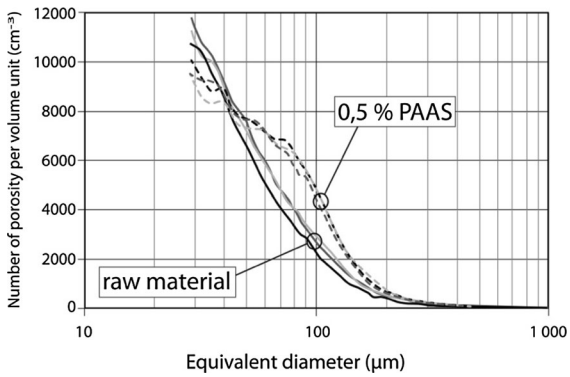

Fig. 7 Volume density versus equivalent diameter of micropores analysed from microtomography

the line is simply drawn to guide the eye. The difference between both series is small but relevant since the dispersion measurement on a given series is clearly smaller. It has been shown in cement that MIP confidence is weak on large diameter equivalent pores (low pressure) and limited to surface pores [17, 30]. These pores correspond to bubbles of entrapped air during the processing which is similar in our present case. Therefore the analysis of the macroporosity has been conducted only on the tomography results. The main differences between both series, is a marked peak with a shoulder on the left part (smaller pore sizes) in the microporosity range. We have considered this range between 1 and 30 µm as a region of interest to calculate the so-called microscopic porosity, and we indeed observe a slight difference between the specimens. Below this porosity range, the difference between both series is not significant on the MIP diagram. Furthermore, within this pore range the drying method is of importance in relation to the pore structure [10, 18, 28]. Classical drying destroys the nano-pore structure and the appropriate methodology is still discussed in the literature. Therefore we do not have access to the porosity at the platelets scale. Hence we propose to evaluate this type of pore content by subtracting the so-called micro porosity obtained by MIP and macro porosity obtained by tomography to the total porosity obtained by MIP and Arthur's method (cf. Table 3). The result, that should be considered with caution, shows that the nanoporosity decreases with the addition of dispersant.

Figure 9a shows three examples of micrographs obtained at two different magnitudes for samples with or without dispersing agent. A difficulty in the analysis of such preparation is that it contains not only clay particles but also particles of illites and quartz. Therefore it is difficult to make the distinction between these particles and flocs of clay platelets. However at low magnification a rougher surface with more pores

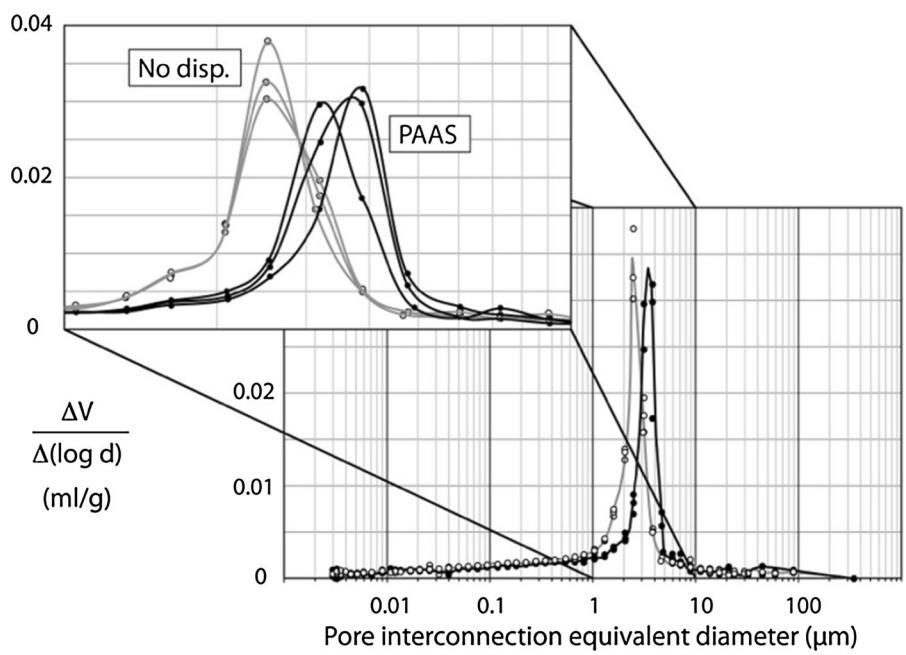

Fig. 8 Pore interconnection distribution measured by mercury intrusion porosimetry. The *solid symbols* represent an average of two samples of a mortar without dispersant, the *empty symbols* represent an average of two mortar samples made with PAAS and HMP dispersants

Table 3 Sample relative porosity summary

Characteristic length	Method	No dispersant (%)	PAA-S (%)	HMP
Total porosity	MIP	25.25	23.20	21.9
	Arthur	23.8	21.3	–
Macroporosity	X-ray tomography	4.4	6.0	n.d.
Microporosity	MIP (partial)	5.65	3.7	n.d.
Nanoporosity	Calculated	15.2	13.5	n.d.

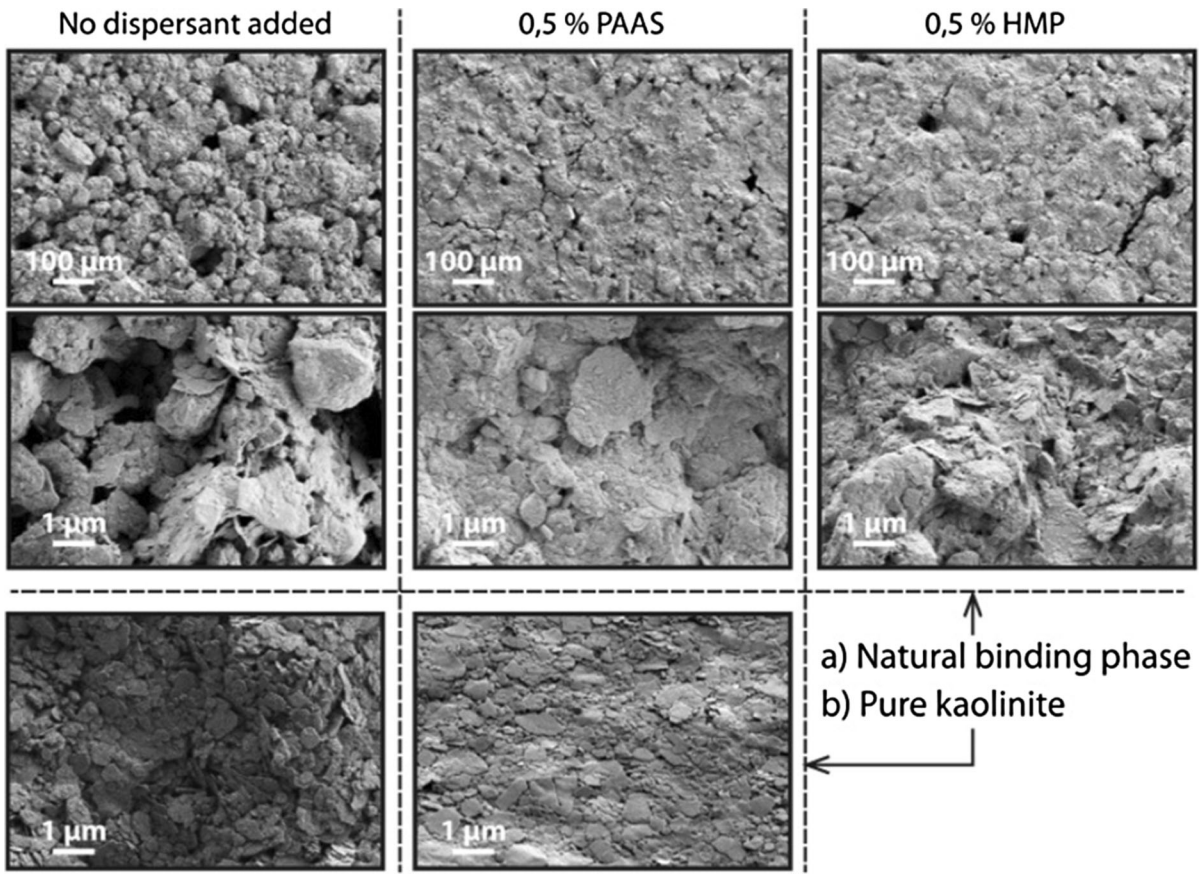

Fig. 9 SEM micrographs of the binder phase without dispersant and with the HMP and PAAS dispersants. A drop of the binding phase in the liquid state was deposited on the microscope stage and observed after drying

is observed on the specimen made without dispersant. This suggests that this specimen is constituted of large flocs, conversely to both specimens without dispersant where finer pores without flocs are observed.

To confirm this assumption a specimen containing "pure" kaolinite clay suspension (BS3 ALSI H from AGS minerals, Imerys group, France) was prepared. The influence of the dispersant on the organisation of the clay platelets can be seen more clearly (Fig. 9b). The dispersion of platelets solely in water is difficult and they define flocs. The addition of a dispersant facilitates a more compact organisation of the platelets, with their face almost parallel to the surface. Clearly this simplified experiment allows a long distance organisation not possible in the mortar suspension, but it can describe the local organisation of the platelets around the sand particles.

3.4 Discussion

The main observations on the addition of a dispersant are a marked increase of the mechanical properties and an evolution of the microstructure described as (i) decrease of flocs, with less entangled clay platelets, (ii) increase of the macro-porosity content and (iii) decrease of the microporosity content. At a first sight, this is surprising since mechanical properties are generally linked to defects and often the largest. In order to get insights in the evolution of the mechanical properties, it is interesting to make a schematic description of the complex microstructure, based on the Rumpf model. The material can be described as a two-scale structure as shown on the schematic drawing in Fig. 10. A so-called macroscopic scale described as a compact of spheres representing the sand bonded by the binding phase, with or without dispersant. The binding phase itself on a microscopic scale is described as a compact of spheres representing the clay platelets and the finest agregate particles bonded by water or weak bonds [42]. At the macroscopic scale, two parameters are of importance for the Rumpf model, the packing density (which appears as $1 - P$ in Rumpf formula) ϕ_{Macro} of this macrostructure and the force f_{Macro} between the sand particles given by the cohesion of the boundary phase. Under a similar description, the microscopic scale, can be described by the packing density ϕ_{micro} and the force between clay particles f_{micro}. The reduction of flocs due to the addition of dispersant increases this latter parameter, and therefore the macroscopic cohesion. This description is confirmed by the different observations. In the case of the mortar we observe an increase of the number of pores in the upper size range between 50 and 300 µm. This means the macro scale packing density ϕ_{Macro} is reduced. This should lead to a decrease of strength, which is the opposite of what we observed. It suggests that the force between aggregates f_{Macro} increases. The augmentation of this force could be due to the increase of the microscopic packing density, i.e. of the bridges between sand particles. This is confirmed by the SEM observations (and the mercury intrusion porosimetry), and this can also be shown by the weak increase of the density with dispersant addition related to the reduction of nano and micro-porosity. Another contribution of this increase of resistance of bridge may arise from the better organisation of the platelets since as previously explained HMP and PAA promote a face-to-face piling up. This contribution is supported by the Van Damme suggestion that shows the dependence of the spatial organization of clay platelets [42]. He has calculated the cohesion of a sand/kaolinite model material as function of the fraction of the kaolinite platelets surface in nearest neighbor situation, and obtained an increasing value with the surface. It can be assumed that the increase of cohesion with dispersant induce the observed increase of strength and elastic modulus of the material.

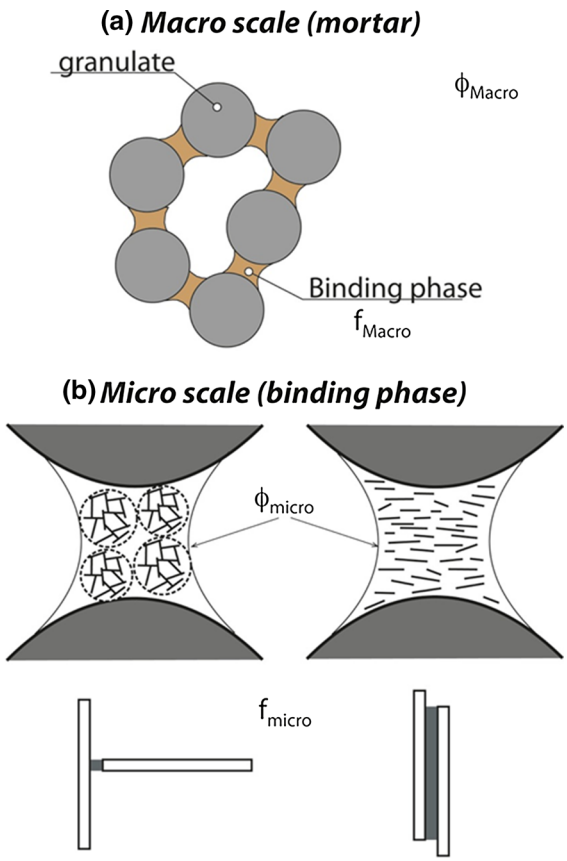

Fig. 10 Schematic drawing of the mortar microstructure

4 Conclusion and perspectives

In the framework of earth construction we have shown that the use of dispersants of different action modes, electrosteric (PAA) and complexing agent (HMP) allow reducing the viscosity. A subsequent interesting result is that the addition of a dispersant, would allow

to reduce the quantity of water used for the dispersion, for a constant workability, therefore a decrease of the drying shrinkage and possibly a faster drying. This would be obtained without degradation of the packing quality, since the dispersants act on the surface. These allow a fist step toward "poured earth" shaping technology, which would dramatically increase the "diffusion" of earth building.

The most important result is a significant increase of the strength of the mortar resulting from an increase of the cohesivity of binding clay bridges, i.e. their cohesive force and their packing density, in terms of the Rumpf model.

In other to obtain a more detailed analysis of the bridge force, nano-scale analysis, such as FIB, TEM and micro-tomography should be conducted. The next step for this work will be to analyse the effect of dispersant addition on the reliability of the earth based strength. Indeed a major drawback of earth construction is the variability of starting materials and therefore the results.

Acknowledgments This work was carried out in the framework of a C2D2 project ≪Béton d'Argile environmental≫, financed by Direction de la Recherche et de l'Innovation du Ministère de l'Écologie, du Développement Durable, des Transports et du Logement.

References

1. Aïtcin P-C (2011) High performance concrete. CRC Press, New-York
2. Anderegg FO (1931) Grading aggregates-II.—the application of mathematical formulas to mortars. Ind Eng Chem 23:1058–1064
3. Andreasen A (1930) Ueber die Beziehung zwischen Kornabstufung und Zwischenraum in Produkten aus losen Körnern (mit einigen Experimenten). Kolloid-Zeitschrift 50:217–228. doi:10.1007/BF01422986
4. Andreasen AM, Jensen W, Lundberg JJV (1929) Ein Apparat für die Dispersoidanalyse und einige Untersuchungen damit. Kolloid-Zeitschrift 49:253–265. doi:10.1007/BF01422732
5. Andreola F, Castellini E, Ferreira J, Olhero S, Romagnoli M (2006) Effect of sodium hexametaphosphate and ageing on the rheological behaviour of kaolin dispersions. Appl Clay Sci 31:56–64
6. Arthur G (1955) Porosity and permeability changes during the sintering of copper powder. J Inst Met 83:329–336
7. Bergaya F, Theng BKG, Lagaly G (2011) Handbook of clay science. Elsevier, Oxford
8. Bowen P, Carry C, Luxembourg D, Hoffmann H (2005) Colloidal processing and sintering of nanosized transition aluminas. Powder Technol 157:100–107. doi:10.1016/j.powtec.2005.05.015
9. Buffiere J, Maire E, Adrien J, Masse J, Boller E (2010) In Situ experiments with X-ray tomography: an attractive tool for experimental mechanics. Exp Mech 50:289–305. doi:10.1007/s11340-010-9333-7
10. Chatterji S (2001) A discussion of the paper "Mercury porosimetry—an inappropriate method for the measurement of pore size distributions in cement-based materials" by S. Diamond. Cem Concr Res 31:1657–1658
11. Chen HYT, Wei WCJ, Hsu KC, Chen CS (2007) Adsorption of PAA on the alpha-Al_2O_3 surface. J Am Ceram Soc 90:1709–1716. doi:10.1111/j.1551-2916.2007.01644.x
12. Chiu R, Cima M (1993) Drying of granular ceramic films: II, drying stress and saturation uniformity. J Am Ceram Soc 76:2769–2777
13. Corradi A, Manfredini T, Pellacani G, Pozzi P (1994) Deflocculation of concentrated aqueous clay suspensions with sodium polymethacrylates. J Am Ceram Soc 77:509–513
14. Cottrino S, Jorand Y, Adrien J, Olagnon C (2013) Spray-drying of highly concentrated nano alumina dispersions. Powder Technol 237:586–593. doi:10.1016/j.powtec.2012.12.058
15. Desset S, Spalla O, Lixon P, Cabanet B (2001) From powders to dispersions in water: effect of adsorbed molecules on the redispersion of alumina particles. Langmuir 17:6408–6418. doi:10.1021/la010166t
16. Di Giuseppe E, D'Orazio M (2014) Moisture buffering "active" devices for indoor humidity control: preliminary experimental evaluations. Energy Procedia. 62:42–51
17. Diamond S (2000) Mercury porosimetry : an inappropriate method for the measurement of pore size distributions in cement-based materials. Cem Concr Res 30:1517–1525
18. Diamond S (2001) Reply to the discussion by S. Wild of the paper "Mercury porosimetry—an inappropriate method for the measurement of pore size distributions in cement-based materials" by S. Diamond. Cem Concr Res 31:1655–1656
19. Doat P (1985) Construire en terre. Editions Alternatives, Paris
20. Gallé C (2001) Effect of drying on cement-based materials pore structure as identified by mercury intrusion porosimetry : a comparative study between oven-, vacuum-, and freeze-drying. Cem Concr Res 31:1467–1477
21. Gelard D (2005) Identification et caractérisation de la cohésion interne du matériau terre dans ses conditions naturelles de conservation. Dissertation, INPG
22. Giesche H (2006) Mercury porosimetry: a general (practical) overview. Part Part Syst Charact 23:9–19. doi:10.1002/ppsc.200601009
23. Kendall K (1988) Agglomerate strength. Powder Metall 31:28–31
24. Kouakou CH, Morel JC (2009) Applied clay science. Appl Clay Sci 44:27–34. doi:10.1016/j.clay.2008.12.019
25. Lagaly G (2005) From clay mineral crystals to colloidal clay mineral dispersions. Coagul Flocculation 2:519–600
26. Lagaly G, Ziesmer S (2003) Colloid chemistry of clay minerals: the coagulation of montmorillonite dispersions. Adv Colloid Interface Sci 100:105–128
27. Laribi S, Fleureau J-M, Grossiord J-L, Kbir-Ariguib N (2005) Comparative yield stress determination for pure and

interstratified smectite clays. Rheol Acta 44:262–269. doi:10.1007/s00397-004-0406-3
28. Lee H (1990) Validity of using mercury porosimetry to characterize the pore structures of ceramic green compacts. J Am Ceram Soc 73:2261–2265
29. Loginov M, Larue O, Lebovka N, Vorobiev E (2008) Fluidity of highly concentrated kaolin suspensions: influence of particle concentration and presence of dispersant. Colloid Surf A 325:64–71. doi:10.1016/j.colsurfa.2008.04.040
30. Moro F (2002) Ink-bottle effect in mercury intrusion porosimetry of cement-based materials. J Colloid Interface Sci 246:135–149
31. Naik TR (2008) Sustainability of concrete construction. Pract Period Struct Des Constr 3:98–103
32. Nordby AS, Shea AD (2013) Building materials in the operational phase. J Ind Ecol 17:763–776
33. Onoda GY, Hench LL, University of Florida (1978) Ceramic processing before firing. Wiley-Interscience, London
34. Quemada D (1998) Rheological modelling of complex fluids. I. The concept of effective volume fraction revisited. Eur Phys J AP 1:119–127
35. Rael R (2009) Earth Architecture. Architectural Press, Princeton
36. Rode C, Peuhkuri RH, Mortensen LH, Hansen KK et al (2005) Moisture buffering of building materials. Department of Civil Engineering, Technical University of Denmark, Kongens Lyngby
37. Rode C, Peuhkuri R, Hansen KK (2005) Moisture buffer value of materials in buildings. Presented at the seminar on moisture buffer capacity in August, pp 1–8
38. Santhiya D, Nandini G, Subramanian S, Natarajan K, Malghan S (1998) Effect of polymer molecular weight on the absorption of polyacrylic acid at the alumina–water interface. Colloid Surf A 133:157–163
39. Schubert H, Herrmann W, Rumpf H (1975) Deformation behaviour of agglomerates under tensile stress. Powder Technol 11:121–131. doi:10.1016/0032-5910(75)80037-4
40. Studart AR, Amstad E, Gauckler LJ (2007) Colloidal stabilization of nanoparticles in concentrated suspensions. Langmuir 23:1081–1090. doi:10.1021/la062042s
41. Tadros TF (2011) Rheology of dispersions. Wiley, Weinheim
42. Van Damme H, Zabat M, Laurent JP (2004) Nature and distribution of cohesive forces in earthen building materials. In: International conference on the conservation of grotto sites; motto grottoes, Dunhuang, pp 1–538
43. Webb P, Orr C (1997) Pore structure by mercury intrusion porosimetry (MIP). Analytical methods in fine particle technology. Micromeritics Instruments Corp., Norcross, pp 155–191
44. Xu L, Helstroom R, Scott O, Chambers AJ (1995) Fracture characteristics of powder compacts. Powder Technol 83:193–199
45. Zaman A, Mathur S (2004) Influence of dispersing agents and solution conditions on the solubility of crude kaolin. J Colloid Interface Sci 271:124–130
46. Zaman A, Tsuchiya R, Moudgil BM (2002) Adsorption of a low-molecular-weight polyacrylic acid on silica, alumina, and kaolin. J Colloid Interface Sci 256:73–78. doi:10.1006/jcis.2001.7941